RSC Advances

PAPER

View Article Online
View Journal | View Issue

Cite this: *RSC Adv.*, 2025, **15**, 31539

Enhanced photodynamic therapy of cancer using porphyrin-based nanoparticles synthesized *via* the co-precipitation method

Punnya Anil Kumar Jeeja,[ab] Atqiya Nafisa,[a] Anh Nguyen,[a] Abbe Eliasof,[a] Audrey Berger,[a] Paula Loman-Cortes[ab] and Juan L. Vivero-Escoto *[ab]

Photodynamic therapy (PDT) is a minimally invasive treatment modality that offers an alternative or supplementary approach to chemotherapy and surgery, characterized by low toxicity and reduced side effects. PDT has been applied to various cancers, often in combination with other therapies to enhance its efficacy. The therapy relies on three main components: a photosensitizer (PS), light of a specific wavelength, and molecular oxygen (O_2). Porphyrins are commonly used PSs due to their favorable properties, but their hydrophobic nature leads to aggregation, reducing their therapeutic effectiveness. To address these challenges, we have synthesized porphyrin-based nanoparticles (PNPs) using a co-precipitation method. Three types of porphyrins, tetraphenylporphyrin (**TPP**), 5-(4-aminophenyl)-10,15,20-triphenyl porphyrin (**ATPP**), and polyhedral oligomeric silsesquioxane (POSS)–**ATPP**, were encapsulated in the nanoparticles. The structural properties of the PNPs were characterized using scanning electron microscopy (SEM), dynamic light scattering (DLS), and ζ-potential measurements. *In vitro* studies in cervical cancer (HeLa) and triple-negative breast cancer (MDA-MB-231) cell lines demonstrated improved internalization and phototherapeutic effects of the PNPs compared to the parent porphyrins. Our findings suggest that encapsulating porphyrins in nanoparticles enhances their photodynamic therapy efficacy, offering a promising approach for cancer treatment.

Received 9th July 2025
Accepted 26th August 2025

DOI: 10.1039/d5ra04916d

rsc.li/rsc-advances

1. Introduction

Photodynamic therapy (PDT) is a minimally invasive localized treatment modality that has emerged as an alternative or supplementary approach to chemotherapy and surgery owing to the low toxicity and acquired resistance and side effects.[1,2] PDT has been applied to many varieties of cancers[3,4] combined with chemotherapy, radiotherapy, immunotherapy and gene therapy to provide a synergistic therapeutic effect in cancer therapy.[5] PDT can directly kill the cancer cells through production of reactive oxygen species (ROS) or depriving circulation of oxygen, activating apoptotic or necrotic cell death pathways.[1,2,4,6] The three main components in PDT are a photosensitizer (PS), light of a specific wavelength and molecular oxygen (O_2).[4] PSs used in PDT are chosen based on their ability to absorb longer wavelength light for deeper penetration, good quantum yield, being inactive in dark and ability to selectively accumulate in tumor tissues with stability and solubility in aqueous solvents.[4,7,8] However, they are generally hydrophobic molecules that are insoluble in aqueous and physiological conditions leading to aggregation of PS in the body.[9] Aggregation prevents cellular internalization as well as inactivates the phototherapeutic properties of the molecules.[7,10,11] The most used photosensitizers are porphyrins, which are considered biodegradable with high extinction coefficients and singlet oxygen quantum yields.[1,4,7,11,12]

In physiological conditions, porphyrins show a reduction of the fluorescence quantum yield and the singlet oxygen production. Moreover, the therapeutic impact is also affected due to low cellular uptake and decrease in the blood circulation time in the body.[4,7,13] Various methods have been introduced to improve the solubility and reduce the aggregation of porphyrin including chemical modification and the use of nanoparticles.[7,8,14,15] Our group has been developing silica-based platforms to improve the delivery and phototherapeutic effect of porphyrins and other photosensitizers. We have used mesoporous silica and polysilsesquioxane nanoparticles to develop efficient carriers with stimuli responsive properties.[16,17] The improved phototherapeutic effect as compared with the parent porphyrin has been demonstrated *in vitro* and *in vivo*.[16,17] Recently, we have reported on the use of polyhedral oligomeric silsesquioxane (POSS) compounds for delivery of porphyrins.[16–18] Our work showed that by tuning the functional groups of POSS an improvement of the phototherapeutic effect was observed. Interestingly, under certain concentrations, the

[a]*Department of Chemistry, University of North Carolina Charlotte, Charlotte, NC, 28223, USA. E-mail: jviveroe@charlotte.edu*

[b]*Chemistry and Nanoscale Science Program, University of North Carolina Charlotte, Charlotte, NC, 28223, USA*

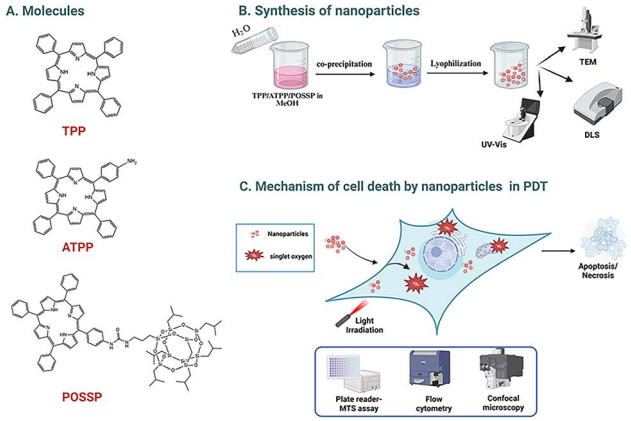

Fig. 1 (A) Three different porphyrins were used in this work: tetraphenylporphyrin (**TPP**), 5-(4-aminophenyl)-10,15,20-triphenyl porphyrin (**ATPP**) and **POSSP**. (B) The co-precipitation method was used to synthesize the PNPs using the parent porphyrin molecules. The physicochemical features of the PNPs were fully characterized. (C) The phototherapeutic performance and cell death mechanisms associated with PNPs were investigated in MDA-MB-231 and HeLa cells.

POSS porphyrin (**POSSP**) molecules with hydrophobic groups performed better than their hydrophilic version.[16,19] This was explained using molecular simulation based on the unique arrangements that are produced by the aggregation of **POSSP**.[18,19] Nevertheless, the performance of these **POSSP** molecules is still suboptimal for PDT applications; therefore, it is appealing to encapsulate these molecules in nanoparticles to improve their PDT effect.

In this work, we have fabricated porphyrin-based nanoparticles (PNPs) using a co-precipitation approach. Three different porphyrins were encapsulated in the nanoparticles: tetraphenylporphyrin (**TPP**), 5-(4-aminophenyl)-10,15,20-triphenyl porphyrin (**ATPP**) and POSS–**ATPP** (**POSSP**) (Fig. 1). The structural properties of the PNPs were characterized using scanning electron microscopy (SEM), dynamic light scattering (DLS) and ζ-potential. The internalization, phototherapeutic effect and cell death mechanisms of the PNPs were investigated *in vitro* using cervical cancer (HeLa) and triple-negative breast cancer (MDA-MB-231) cell lines. Our results demonstrated that by encapsulating the parent porphyrins in PNPs a better phototherapeutic effect as compared with the parent porphyrins is obtained.

2. Experimental

2.1 Materials

Tetraphenylporphyrin (**TPP**) was obtained from Tokyo Chemical Industry, 5-(4-aminophenyl)-10,15,20-triphenyl porphyrin (**ATPP**) was obtained from Frontier Scientific, trisilanol isobutyl POSS from WL Runnels Industrial Drive, carbodiimide (EDC) was purchased from Oakwood Chemical. Diethyl ether, dichloromethane (DCM), methanol, acetonitrile, ether, DIPEA and triphosgene, tetramethyl ammonium hydroxide (TMAOH) and the rest of the chemicals used in this work were obtained from Sigma-Aldrich and VWR Chemicals. All the reagents were used without any further purification unless specified otherwise. Nanopure water of 17.6 MΩ cm was used. A homemade LED device emitting at 630 nm (fluence rate = 116.33 mW cm^{-2}) was used for our *in vitro* experiments (Laboratory of Technological Support, São Carlos Institute of Physics, Brazil). Roswell Park Memorial Institute (RPMI 1640), penicillin–streptomycin (pen–strep), phosphate buffer saline (PBS, 1×), and trypsin were purchased from Corning. 2′,7′-dichlorodihydrofluorescein diacetate (DCFH-DA) was purchased from Sigma-Aldrich. CellTiter 96® Aqueous Assay was obtained from Promega (Madison, WI, USA). Fetal bovine serum (FBS) was purchased from Atlanta Biologicals. Hoechst 33342 dye was purchased from Life Technologies. Sterile-filtered DMSO was used for all cell experiments and purchased from Sigma. BD Pharmingen™ Annexin V-FITC Apoptosis Detection Kit was purchased from BD Biosciences. SYTOX™ Blue dead cell stain was purchased from Thermo Fisher Scientific USA.

2.2 Methods

2.2.1 Synthesis of hepta(isobutyl)-POSS-porphyrin (5-(4-[3-(3-(3,5,7,9,11,13,15-heptaisobutyl pentacyclo[9.5.1.1(3,9).1(5,15).1(7,13)]octasiloxane)propyl)ureido]phenyl)-10,15,20-(triphenyl)porphyrin) (POSSP). The synthesis of **POSSP** has been previously reported and consists of a three-step reaction including functionalization of POSS with aminopropyl groups, conversion of the amino to isocyanato groups and reaction with **ATPP**.[18,19] Briefly, trisilanol hepta(isobutyl) POSS (1.00 g, 1.26 mmol) was dispersed in ethanol (6.25 mL) while being stirred at 550 rpm, and then TMAOH (20 μL, 0.03 mmol, 25% w/v) and APTES (212 μL, 217.5 mg, 0.985 mmol) were added. The mixture was stirred for 43 h (700 rpm) at 40 °C. During the reaction period, a significant quantity of aminopropyl hepta(isobutyl) POSS precipitated. After centrifuging at 1300 rpm for 15 min the dispersion, the supernatant was discarded. Acetonitrile was used to wash the solid product twice under the same conditions. The product was vacuum-dried for 48 h (yield = 84% wt).

The procedure for synthesizing isocyanato propyl hepta(-isobutyl) POSS was carried out by mixing aminopropyl hepta(-isobutyl) POSS (75 mg, 0.086 mmol) with dry dichloromethane (1 mL) at room temperature. After that, the mixture was stirred slowly (300 rpm) under nitrogen atmosphere. Then, DIPEA (30 μL, 22.25 mg, 0.17 mmol) and triphosgene (12.75 mg, 0.043 mmol) were added to this solution. The solvent was allowed to evaporate for 10 min after 3 h by increasing the nitrogen flow and stirring rate (800 rpm). After precipitation was complete, the mixture was centrifuged for 15 min at 1300 rpm to remove the supernatant. Acetonitrile was used to wash the product twice. The product was vacuum-dried for 48 h (yield = 84% wt).

Finally, isocyanato propyl hepta(isobutyl) POSS (10 mg, 0.011 mmol) was dissolved in 1 mL of dry dichloromethane at room temperature. To this solution excess of DIPEA (120 μL) and 5-(4-aminophenyl)-10,15,20-(triphenyl) porphyrin (**ATPP**) (14 mg, 0.0225 mmol) was added. In a sealed flask, the final solution was stirred (400 rpm) at room temperature for 48 h under dark.

Using column chromatography on silica gel (ether : MeOH; 99 : 1), the product was separated. After purification, **POSSP** was dried and obtained as a dark powder (yield = 82% wt).

2.2.2 Synthesis of ATPP or TPP nanoparticles. A solution of 0.333 mM of **ATPP** or **TPP** in chloroform was made by dissolving 10.5 mg of **ATPP** or 10.25 mg of **TPP** in 50 mL of chloroform in a 50 mL volumetric flask. The solution was sonicated for 5 min to ensure all **ATPP** or **TPP** was dissolved. In a 20 mL scintillation vial, 5.0 mL of methanol were added followed by 0.20 mL of the **ATPP** or **TPP** solution in chloroform. The vial was gently swirled to ensure the **ATPP** or **TPP** solution mixed with the MeOH. Over the course of 1 min, 10 mL of nanopure H_2O was added dropwise to the vial. Every 10 seconds during the H_2O addition, the vial was gently swirled. The vials were allowed to remain open for a week and kept at room temperature to allow the evaporation of volatile solvents. After the evaporation of MeOH, the vials were transferred into 50 mL centrifuge tubes and lyophilized for a week to remove water and obtained brownish solid nanoparticles. After that, 0.50 mL of water was added to each centrifuge tube and 4 tubes were combined into a 25 mL centrifuge tube.

2.2.3 Synthesis of POSSP nanoparticles. A solution of 0.333 mM **POSSP** in chloroform was made by dissolving 25.48 mg of **POSSP** in 50 mL of chloroform in a 50 mL volumetric flask. The solution was sonicated for 5 min to ensure all **POSSP** was dissolved. A 20 mL scintillation vial was charged with 5.0 mL of MeOH. After the methanol, 1.0 mL of the **POSSP** solution was added. The vial was gently swirled to ensure the **POSSP** solution mixed with the MeOH. Over the course of 10 seconds, 1.0 mL of nanopure H_2O was added to the vial. The vials were allowed to remain open for a week and kept at room temperature to allow the evaporation of volatile solvents. After the evaporation of MeOH, ten vials were combined into 50 mL centrifuge tubes and lyophilized for a week to remove water and obtained brownish solid nanoparticles.

2.2.4 Characterization of POSSP molecules. POSSP was characterized using FT-IR (PerkinElmer 100 IR) spectrophotometer from 4000 to 700 cm^{-1} (Waltham, MA, USA), ^{1}H-NMR (300 MHz JEOL NMR spectrometer (Peabody, MA, USA)) and MALDI-TOF (Voyager Biospectrometry Laser).

2.2.5 Characterization of TPP-, ATPP- and POSSP-NPs

Hydrodynamic diameter, ξ-potential and colloidal stability. To determine the hydrodynamic size and ξ-potential of **TPP-**, **ATPP-** and **POSSP**-NPs, the nanoparticles were dispersed in water at a concentration of 0.1 mg mL^{-1}. The resultant dispersion was incubated at room temperature for 30 min before analysis using a Malvern Zetasizer nano. Measurements were conducted at 20 °C with a 2 min equilibration step between each subsequent measurement. The colloidal stability of the nanoparticles was done at a concentration of 0.1 mg mL^{-1}. The size and polydispersity index were measured for 12 h in the Malvern Zetasizer nano to see the variation to indicate colloidal stability.

Absorbance. The absorbance of **TPP-**, **ATPP-** and **POSSP**-NPs synthesized were characterized in nano pure water by Cary 5000 UV-vis-NIR spectrophotometers, respectively.

2.2.6 Cell culture. Human cervical carcinoma (HeLa) and triple-negative breast (MDA-MB-231) cancer cell lines were purchased from the American Type Culture Collection (ATCC, USA). HeLa and MDA-MB-231 cells were cultured in Roswell Park Memorial Institute (RPMI 1640, Thermo Fisher Scientific, Waltham, MA, USA) supplemented with 10% fetal bovine serum (Thermo Fisher Scientific), 1% penicillin/streptomycin (HyClone, Logan, UT, USA), Cells were incubated in a humidified atmosphere of 5% CO_2 at 37 °C.

2.2.7 Cellular uptake of PNPs. To evaluate the cellular uptake **TPP-**, **ATPP-** and **POSSP**-NPs, HeLa and MDA-MB-231 cell lines were cultured at a density of 2.0×10^5 and 2.5×10^5 cells per well respectively, in a 6-well plate containing 1 mL of RPMI media. The corresponding molecules in RPMI media were prepared from a stock of 20% DMSO-nanopure water solution. The cells were maintained for 24 h at 37 °C with 5% CO_2 in a humidified incubator. Cells were then treated with PNPs at concentration of 400 μM and incubated for 24 h at 5% CO_2 atmosphere at 37 °C. Afterwards, the cells were washed with phosphate buffer, followed by detachment of cells using 0.25% trypsin–EDTA. The cells were then suspended in DBPS for analysis with the flow cytometer (BD LSR™ cell analyzer) using PE-Texas red channel.

2.2.8 Phototoxicity assessment. HeLa (1×10^4 cells per well) and MDA-MB-231 cells (2×10^4 cells per well) were seeded into 96-well plates and incubated for 24 h at 37 °C with 5% CO_2 in a humidified incubator. After that, the cells were treated with various concentrations ranging from 100 to 1000 μM of **TPP**, **ATPP**, **POSSP** molecules or the corresponding PNPs. The PNPs in media were prepared from a stock of nanopure water whereas the molecules from 20% DMSO nanopure water solution. The cells were incubated in the presence of molecules or PNPs for 48 h at 37 °C. Next, cells were washed once with cold DPBS followed by irradiation with red light ($\lambda = 630$ nm, fluence rate = 116.33 mW cm^{-2}) for 20 min in cold DPBS. DPBS was aspirated and cells were resuspended in complete RPMI and incubated at 37 °C for an additional 24 h. Subsequently, cells were incubated at 37 °C with 20% v/v of the cell titer 96 MTS solution in complete RPMI for 150 min. As a dark control experiment, an unirradiated duplicate plate was maintained for each treatment condition. Cell viability was determined by analyzing absorbance values recorded at 490 nm using a Multiskan microplate reader. Cell viability (%) was calculated as follows: viability = $(A_{sample} - A_{blank})/(A_{control} - A_{blank}) \times 100\%$, where A_{sample}, $A_{control}$ and A_{blank} denote absorbance values of the sample, control, and blank wells. The IC_{50} values are determined using Origin (v2.1 for Windows, La Jolla, CA, USA), fitting the normalized viability data to a nonlinear regression.

2.2.9 Apoptosis experiments. HeLa and MDA-MB-231 cells were seeded in 6 well plates at a density of 2.0×10^5 and 2.5×10^5 cells per well respectively and incubated at 37 °C for 24 h with 5% CO_2 in a humidified incubator. After that, the cells were treated with porphyrin molecules or PNPs at a concentration of 400 μM and incubated for 24 h. Then, the cells were washed once with cold DPBS and irradiated with red light ($\lambda = 630$ nm, fluence rate = 116.33 mW cm^{-2}) for 20 min in cold DPBS. The solution was aspirated, and cells were resuspended in complete RPMI and incubated at 37 °C for an additional 24 h. After that, cells were collected by trypsinization and resuspended in 200 μL

of 1× binding buffer. To this dispersion, 1 μL of FITC tagged annexin V was added and incubated for 10 min, followed by 0.5 μL of SYTOX Blue dead cell dye was added and incubated for another 5 min. The final volume was brought up to 500 μL by adding 300 μL of binding buffer. The cells were analyzed by flow cytometry (BD Fortessa) for FITC-annexin V and SYTOX Blue positive population. Unstained cells, FITC-annexin and SYTOX Blue stained blank cells were seeded in each plate and used to determine the background fluorescence as control.

2.2.10 Confocal experiments for internalization. HeLa and MDA-MB-231 cells were seeded in 6 well plates with cover glass at a density of 5×10^3 cells per well and 1×10^4 cells per well respectively and incubated at 37 °C for 24 h with 5% CO_2 in a humidified incubator. Cells were treated with porphyrin molecules or PNPs at concentration of 400 μM. After 24 h, cells were washed once with cold DPBS. Two drops of nuclei staining dye were added to each well and let it sit in the biosafety cabinet for 15 min. Finally, the cover glass was transferred to a glass slide for confocal experiments. Olympus Fluoview FV 1000 was used to obtain confocal images.

2.2.11 Confocal experiments for ROS generation. HeLa and MDA-MB-231 cells were seeded in 6 well plates at a density of 5×10^3 cells per well and 1×10^4 cells per well respectively and incubated at 37 °C for 24 h with 5% CO_2 in a humidified incubator. Cells were treated with porphyrin molecules and nanoparticles at concentration equivalent to the IC_{50} values of the respective materials. After 24 h of inoculation, cells were washed once with cold DPBS and incubated in serum free media containing 10 μM of DCFDA for 1 h at 37 °C in the dark. Then, cells were washed twice with DPBS and irradiated with red light ($\lambda = 630$ nm, fluence rate = 116.33 mW cm^{-2}) for 20 min in cold DPBS. Two drops of nuclei staining dye were added to each well and let it sit in the biosafety cabinet for 15 min. Finally, the cover glass was transferred to a glass slide for confocal experiments. Olympus Fluoview FV 1000 was used to obtain confocal images.

2.2.12 Statistics. All the experimental results in the manuscript are reported as mean ± standard deviation (SD) unless mentioned otherwise. The hydrodynamic size and ξ-potential were carried out in at least triplicates. Cellular uptake and apoptosis assay was evaluated and quantified in triplicates. Cell viability studies were analyzed using Origin Pro 2025 to determine the IC_{50} ($n = 3$). Statistical analysis was evaluated using a one-way ANOVA, followed by a Tukey's multiple comparison test and Bonferroni test. All the statistical analysis was performed using Origin Pro 2025 with a p-value < 0.05 considered to be statistically significant.

3. Results and discussion

3.1 Synthesis and characterization of the POSSP molecule

The synthesis of the **POSSP** molecule was carried out following a three-step approach reported in the literature.[18] The protocol comprises the functionalization of POSS with aminopropyl groups, followed by the conversion of the amino to isocyanato groups and finally the reaction of this POSS derivative with the porphyrin (**ATPP**) to afford **POSSP**. The final product was characterized at each step of the process using FT-IR, ^{1}HNMR and MALDI-MS (Fig. S1). The FT-IR shows the successful synthesis of **POSSP** according to the stretching vibrations at (cm^{-1}): 2959 (N–H), 2924 and 2870 (C–H), 1640 (C=O), 1465 (C–N), 1229 (Si–C), 1083 (Si–O–Si), 957 (Si–O–Si), 741 (Si–C). In a similar way, ^{1}HNMR indicates the presence of 8.90 (m, 8H, Py–H), 8.10 (m, 8H, Ph–H), 7.90 (m, 11H, Ph–H), 3.23 (t, 2H, –CH2–N–), 1.88 (m, 7H, –CH–), 1.76 (m, 2H, –CH2–), 0.96 (d, 42H, CH3), 0.71 (t, 2H, –Si–CH2–), 0.61 (m, 14H, -Si –CH2–).Finally, MALDI-MS confirms the presence of **POSSP** by (m/z): $[M-1]^+ =$ 1527.55 observed; $[M]^+ = 1528.55$. As shown in our previous work, the S- and Q-bands of **POSSP** are slightly blue-shifted with respect to their parent porphyrin, **ATPP**[18,19] (Fig. S2 and Table S1).

3.2 Synthesis and characterization of porphyrin-based NPs

In this work, three porphyrins were used as precursors for the synthesis of PNPs : **TPP**, **ATPP** and **POSSP**. The fabrication of the porphyrin-based nanoparticles was performed using a co-precipitation approach.[18] This method relies on the principle of precipitating multiple components simultaneously from a solution. In our case, the PNP precursor was completely dissolved in chloroform followed by its dilution in methanol, both organic solvents are miscible. The dropwise addition of water, followed by the slow evaporation of chloroform and methanol, affords the formation of PNPs (Fig. 2A). The as-synthesized nanoparticles were characterized by DLS, ζ-potential, and SEM. The hydrodynamic diameters of **TPP**-, **ATPP**- and **POSSP**-NPs in water are 459 ± 3, 590 ± 9, 169.9 ± 1 nm ($n = 3$), respectively (Fig. 2B). These data show aggregation of PNPs in aqueous solution as expected because the NPs consist of porphyrin molecules. Interestingly, **POSSP**-NPs showed the lowest hydrodynamic diameter, most likely due to the presence of silica-based POSS component. The ζ-potential of the nanoparticles indicates a negative charge on the surface of the PNPs with values of −49.5 ± 1.7, −46.0 ± 1.1, and −35.4 ± 2.8 mV for **TPP**-, **ATPP**- and **POSSP**-NPs, respectively ($n = 3$) (Fig. 2C). The negative ζ-potential arises from the interaction of exposed π electron clouds in the head to tail arrangement of porphyrin J-aggregates with the aqueous medium.[20–24] The high negative charge also ensure stability in aqueous solution due to electrostatic repulsion.[20,21] SEM shows that the **TPP**-, **ATPP**- and **POSSP**-NPs are spherical in shape with a diameter of 42.0 ± 5.7, 66.0 ± 4.1 and 40.0 ± 5.6 nm ($n = 50$), respectively (Fig. 2D–F).

To have a better understanding of the colloidal stability of the PNPs at longer time, we measured the hydrodynamic diameter and the polydispersity index (PDI) for the PNPs during 12 h in water (Fig. 2G–I). **TPP**- and **ATPP**-NPs showed the largest hydrodynamic diameter > 1000 nm with PDI values close to 1.0. These results confirmed that the presence of the porphyrin molecules results in a high aggregation for these PNPs. However, **POSSP**-NPs present a hydrodynamic diameter of 250 nm at the beginning of the experiment that decreases around 200 nm after 12 h (Fig. 2I). In addition, the PDI values maintain an average of 0.4, which is still acceptable. This is certainly a contribution of the POSS moiety as shown in

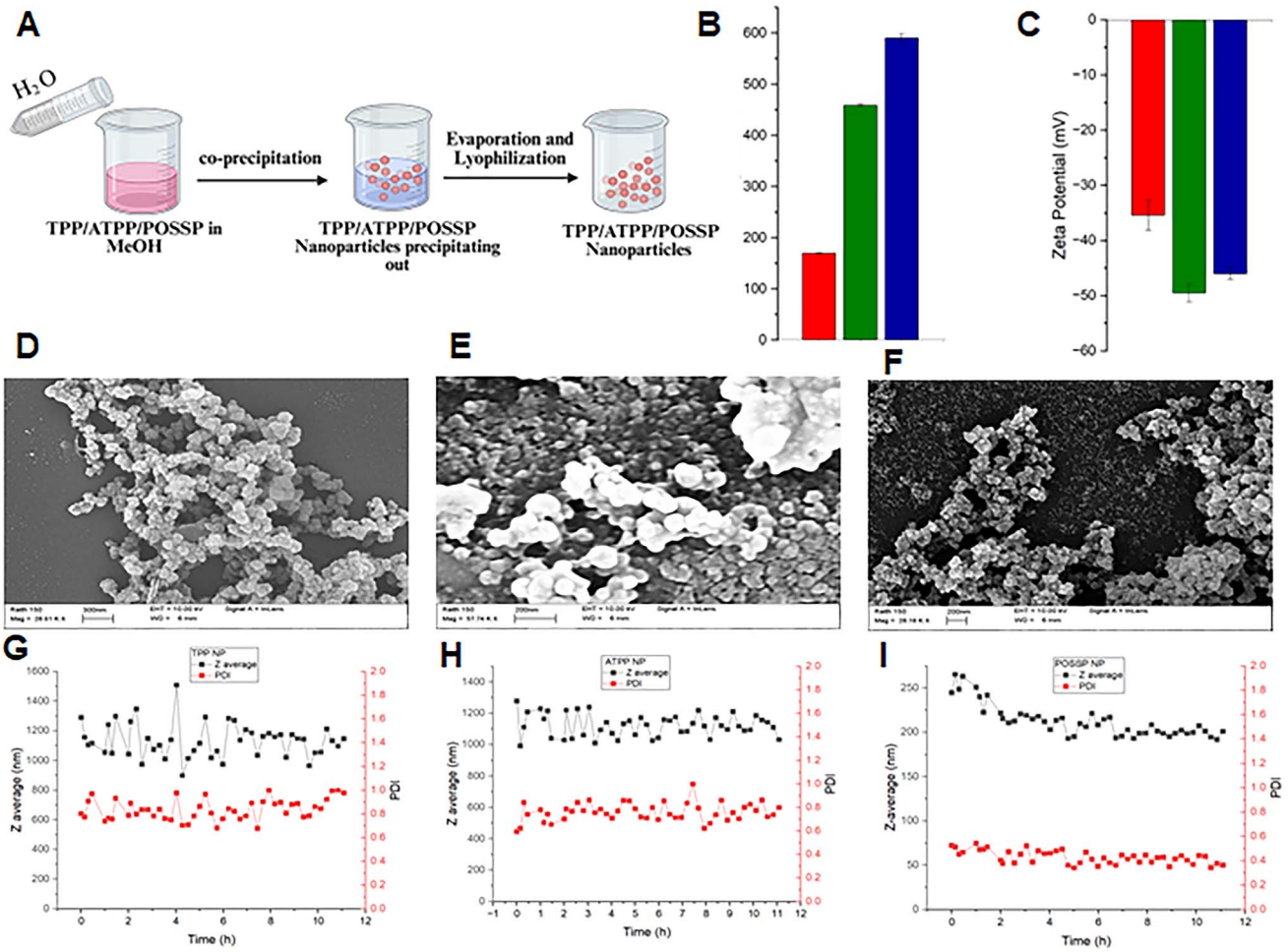

Fig. 2 (A) Synthetic scheme for the fabrication of PNPs using the co-precipitation method. (B) Hydrodynamic diameter and (C) ζ-potential for **POSSP** (red), **TPP** (green) and **ATPP** (blue) nanoparticles. SEM images of (D) **TPP** (42.0 ± 5.7 nm, $n = 50$), (E) **ATPP** (66.0 ± 4.1 nm, $n = 50$) and (F) **POSSP** (40.0 ± 5.6 nm, $n = 50$) nanoparticles. Colloidal stability in simulated physiological conditions (PBS 1 mM, pH 7.4, RT) of (G) **TPP**, (H) **ATPP** and (I) **POSSP** nanoparticles.

previous publications that presence of the silica-based polysilsesquioxane nanocarriers improves the colloidal stability of the hydrophobic porphyrins by entrapping them and increasing the water solubility, thus reducing the aggregation.[16,17]

3.2.1 Photophysical characterization of PNPs. The UV-vis absorbance of the nanoparticles in aqueous solution shows maximum absorbance between 400–450 nm corresponding to the Soret-band of the parent porphyrins (Fig. S2). The corresponding Q-bands from porphyrins are also present in the PNPs at the following wavelengths 510–530, 545–565, 585–595 and 645–660 nm. Interestingly, there is a red shift observed in all the PNPs as compared with their corresponding parent porphyrin molecules (Table S1). Red shifts of 3.5, 6.0 and 4.5 nm were observed for **TPP**-, **ATPP**- and **POSSP**-NPs, respectively. Red shift is typically related to J-aggregation, which indicates that the porphyrin monomers are aligned head-to-tail.[20,25–29] This provides evidence for reduction in porphyrin aggregation in nanoparticles, which can improve the solubility in physiological conditions. Improved photoactivity can also be achieved with reduced aggregation (Fig. S2).[20,25,26,29,30]

3.3 *In vitro* characterization of porphyrin-based NPs

3.3.1 Internalization of porphyrin-based nanoparticles. The internalization of **TPP**-, **ATPP**- and **POSSP**-NPs was evaluated in HeLa and MDA-MB-231 cells. As PDT is currently used in the treatment of early cervical cancer, HeLa was chosen as a candidate for the phototoxicity studies.[31,32] MDA-MB-231, which is a triplet-negative cancer cell line, was selected because PDT has been explored as an alternative treatment in breast cancer therapies.[33,34] HeLa or MDA-MB-231 cells were inoculated with PNPs at an equivalent concentration of porphyrin of 400 μM for 24 h. The internalization of PNPs was determined by flow cytometry using the fluorescence of the respective porphyrins. In the case of HeLa cells, the percentage of cells that have internalized **ATPP**-, **TPP**- and **POSSP**-NPs was 33.1 ± 2.7, 68.1 ± 9.1 and 19.7 ± 4.3%, respectively (Fig. 3A). The parent porphyrins were used as control, the internalization for **ATPP**, **TPP** and **POSSP** molecules was 0.4 ± 0.3, 1.1 ± 0.6 and 3.1 ± 0.7%, respectively. In the case of MDA-MB-231 cells, the percentage of positive cells for **ATPP**-, **TPP**- and **POSSP**-NPs was 7.5 ± 2.6, 29.2 ± 5.2 and 8.4 ± 2.8%, respectively (Fig. 3E). The internalization for the parent

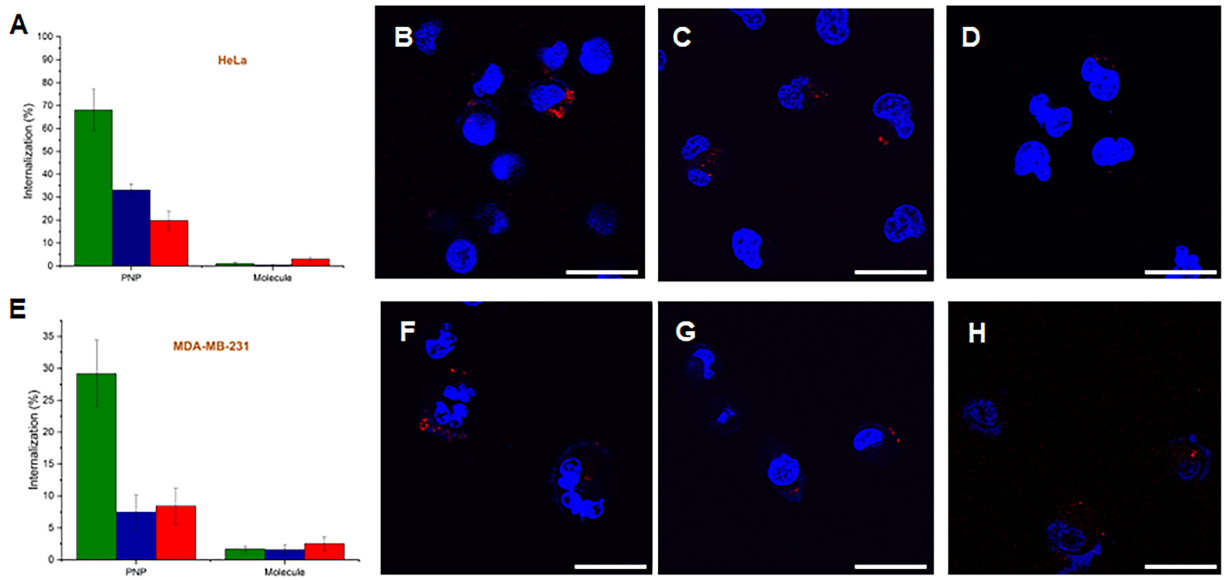

Fig. 3 Quantification of the internalization of PNPs and molecules in (A) HeLa and (E) MDA-MB-231 cells using flow cytometry for **TPP** (green), **ATPP** (blue), **POSSP** (red). Confocal images of internalization of (B) **TPP**-NP (C) **ATPP**-NP and (D) **POSSP**-NP in HeLa cells; and (F) **TPP**-NP (G) **ATPP**-NP and (H) **POSSP**-NP in MDA-MB-231 cells. Blue represents the DAPI-stained nuclei and red show the fluorescence associated with PNPs. Scale bar = 20 μm.

porphyrins **ATPP**, **TPP** and **POSSP** was 1.6 ± 0.8, 1.7 ± 0.4 and 2.5 ± 1.1%, respectively. These results demonstrated that the encapsulation of the porphyrin molecules into nanoparticles enhanced their cellular internalization. A similar trend was observed in both cells with higher internalization of **TPP**-NPs followed by **ATPP**- and **POSSP**-NPs. It is reported that porphyrins with phenyl and alkyl derivatives gets internalized better due to their higher affinity to serum albumin that assists in internalization through endocytosis.[35] The differences in internalization between HeLa and MDA-MB-231 cell lines are most likely attributed to the fastest growth of HeLa cells as compared with MDA-MB-231 which was observed during experiments.

Confocal microscopy was used to confirm the internalization of **ATPP**-, **TPP**- and **POSSP**-NPs in HeLa and MDA-MB-231 cell lines (Fig. 3B–D and F–H). DAPI was used to stain nucleus and red fluorescent indicator porphyrin was utilized as indicator of the nanoparticle presence. The internalization of PNPs was confirmed by the red spots inside the cell body for all the PNPs.

3.3.2 Phototoxicity of porphyrin-based nanoparticles. The photocytotoxicity of **TPP**-, **ATPP**- and **POSSP**-NPs in the presence of light was determined in MDA-MB-231 and HeLa cell lines. A red-light source (λ = 630 nm, fluence rate = 116.33 mW cm^{-2}) was utilized to irradiate the cells for 20 min (139.6 J cm^{-2}). In the case of HeLa cells, the EC_{50} for PNPs in the presence of light was 560.9 ± 37.6, 297.0 ± 10.0, 503.7 ± 2.3 μM for **TPP**-, **ATPP**- and **POSSP**-NPs respectively (Fig. 4A, B and Table S2). These values indicate that **ATPP**-NPs are almost twice more efficient to kill HeLa cells as compared with the other two PNPs. Control experiments with the parent porphyrin molecules in the presence of light did not reach the EC_{50} at the highest concentration used in the experiment for **TPP** and **POSSP** molecule (Table S2 and Fig. S3). However, **ATPP** produced a photocytotoxic effect with a EC_{50} value of 576.7 ± 59.3 μM. This indicates that by encapsulating the porphyrin molecules in nanoparticles the phototherapeutic performance is enhanced. Control experiments of the PNPs in dark conditions showed cytotoxic effects for **ATPP**- and **POSSP**-NPs with EC_{50} values of 643.7 ± 28.5 and 627.1 ± 13.8 μM. Previous research shows that porphyrins are almost nontoxic under dark conditions,[36] however, there are instances where overaccumulation of porphyrin leading to dark toxicity due to redox vulnerability.[37,38] The molecules in dark

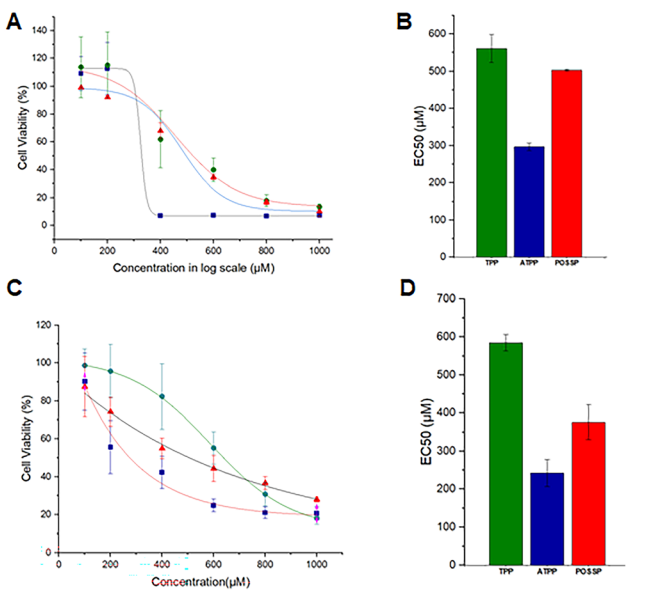

Fig. 4 Drug–response plots for the phototoxicity of PNPs in (A) HeLa and (C) MDA-MB-231 cells under light conditions (λ = 630 nm, fluence rate = 116.33 mW cm^{-2}; 139.6 J cm^{-2}). EC_{50} values obtained for the phototoxicity of **TPP**-NP (green), **ATPP**-NP (blue), **POSSP**-NP (red) for (B) HeLa and (D) MDA-MB-231 cells.

conditions did not show any cytotoxicity at the maximum concentration of 1000 μM tested in these experiments.

In the case of MDA-MB-231 cells, the EC_{50} values for PNPs in the presence of light was 584.9 ± 21.5, 242.3 ± 36.0, 376.2 ± 45.5 μM for **TPP**-, **ATPP**- and **POSSP**-NPs, respectively (Fig. 4C, D and Table S3). The phototoxic performance of PNPs in MDA-MB-231 cells follows the same trend as the one described above for HeLa cells. Control experiments with the parent porphyrin molecules in the presence of light did not reach the EC_{50} at the highest concentration used in the experiment for **TPP** and **POSSP** molecules (Table S3 and Fig. S3). However, **ATPP** produced a photocytotoxic effect with a EC_{50} value of 537.8 ± 27.6 μM. Control experiments of the PNPs in dark conditions showed cytotoxic effects for **TPP**-, **ATPP**- and **POSSP**-NPs with EC_{50} values of 874.8 ± 263.4, 517.7 ± 27.5 and 650.5 ± 117.2 μM. As mentioned before, redox vulnerability could be a cause for this observed toxicity.[37,38] However, the cytotoxicity of the PNPs in the presence of light is still more significant with at 50% more killing effect. The molecules in dark conditions did not show any cytotoxicity at the maximum concentration of 1000 μM tested in these experiments.

Overall, the phototoxicity of the PNPs in HeLa and MDA-MB-231 cells follows the order of **ATPP**-NPs > **POSSP**-NPs > **TPP**-NPs. The highly toxic effect of **ATPP** and **ATPP**-NPs is most likely due to the presence of the amine group which allows the localization of the porphyrin in key organelles.[35,39] It has also been reported that porphyrins with amine groups (NH_2) affect cell adhesion and migration along with binding to telomeres of DNA preventing their elongation, thus enhancing the phototoxicity effect compared to non-cationic porphyrins.[36] This explains the enhanced phototoxicity of **ATPP**-NPs followed by **POSSP**-NPs and toxicity of **ATPP** molecule, although **POSSP**-NPs have a better colloidal stability. It is also important to point out that despite **TPP**-NPs showing the highest internalization, **ATPP**- and **POSSP**-NPs have a better phototoxic performance as an indication that not only internalization is the key factor for the phototherapeutic effect of these nanoparticles.[35,39] Moreover, other studies have demonstrated that at meso and β derivatives showed superior organelle targeting.[35,40,41] In particular, amphiphilic cationic ones showed increased mitochondrial accumulation due to its electrochemical potential leading to cell death. In contrast, **TPP** and anionic derivatives preferentially localize in lysosome causing delayed release and phototoxicity.[35,40] Other than **ATPP**, the other porphyrin molecules did not show any toxicity under the dark conditions (Tables S2 and S3).

3.3.3 Reactive oxygen species generation. To qualitatively confirm that PNPs generate singlet oxygen *in vitro*, DCFH-DA, a ROS probe was used. DCHF-DA gets deacetylated by cellular esterase forming DCFH, which reacts with ROS forming a green fluorescent derivative of dichlorofluorescein.[42] The generation of ROS *in vitro* was determined by confocal microscopy on HeLa and MDA-MB-231 cells. These cells were inoculated with **TPP**-, **ATPP**- and **POSSP**-NPs, irradiated for 20 min as indicated in the experimental section and images were taken using a confocal microscope (Fig. 5). The green fluorescence indicates qualitatively the presence of ROS confirming the generation of ROS inside the cells after light irradiation.

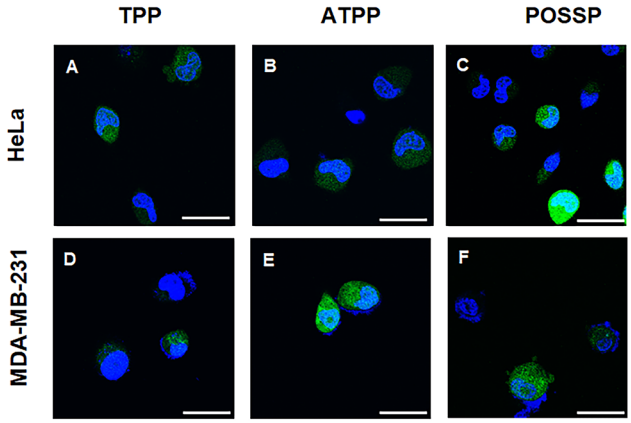

Fig. 5 Confocal images *in vitro* to determine the ROS generation in HeLa or MDA-MB-231 cells using PNPs. (A and D) **TPP**-NP, (B and E) **ATPP**-NP and (C and F) **POSSP**-NP. Blue represents the DAPI-stained nuclei and green shows the ROS generation by PNPs using DCF green fluorescence. Scale bar = 20 μm.

3.3.4 Apoptosis/necrosis. There are typical cell death mechanisms by which porphyrin-mediated PDT works including apoptosis, necrosis, autophagy and ferroptosis.[13,16] Among them, apoptosis is the most common cell death mechanism followed by necrosis.[13,16,43] The ROS generated by porphyrin along with the molecule activates pathways like p38, PERK and p53 leading to apoptosis and necrosis.[13,43] Photosensitizer trapped in the cell membrane or lysosome also triggers necrosis.[13]

To determine the percentage of apoptosis associated with PNPs, we performed apoptosis/necrosis experiments using annexin V assay with HeLa and MDA-MB-231 cells (Fig. 6A). Necrosis was observed as part of the cell death mechanisms for PNP-mediated PDT; however, its contribution is considerably less significant than that of apoptosis (Fig. S4). In HeLa cells, **ATPP**-, **POSSP**- and **TPP**-NPs triggered 62.5 ± 6.0, 39.9 ± 8.5 and 15.1 ± 3.7 percentage of positive cells for apoptosis. In the case of MDA-MB-231 cells, **ATPP**-, **POSSP**- and **TPP**-NPs triggered 38.0 ± 4.7, 9.3 ± 5.9 and 8.8 ± 0.9 percentages of positive cells for apoptosis (Fig. 6F). Flow cytometry data showed that the apoptotic effect of PNPs on HeLa and MDA-MB-231 cells follow the same trend as the phototoxicity experiments with **ATPP**-NPs > **POSSP**-NPs > **TPP**-NPs. The percentage of apoptosis is higher for **ATPP** and **POSSP** NP for both cell lines compared to **TPP**. This confirms the better efficiency of **ATPP** and **POSSP**-NPs to kill the cancer cells by triggering apoptosis cell death pathways. In HeLa cells, **ATPP**, **POSSP** and **TPP** molecules lead to 50.1 ± 2.8, 20.4 ± 2.5 and 19.4 ± 0.7 percentage of apoptosis, respectively (Fig. 6A). These values indicate the efficiency of the corresponding NPs in achieving apoptosis mediated cell death.

MDA-MB-231 cells showed even lower rates of cell death with molecules than the HeLa cells. **ATPP**, **POSSP** and **TPP** molecules led to 10.7 ± 0.4, 12.6 ± 1.3 and 13.2 ± 7.3 percentage of apoptosis, respectively (Fig. 6F). Except **ATPP**, **POSSP** and **TPP** molecules have statistically similar percentages of apoptosis. Both the cell lines have a low percentage of necrotic cell death with nanoparticles and molecules (Fig. 6B and G).

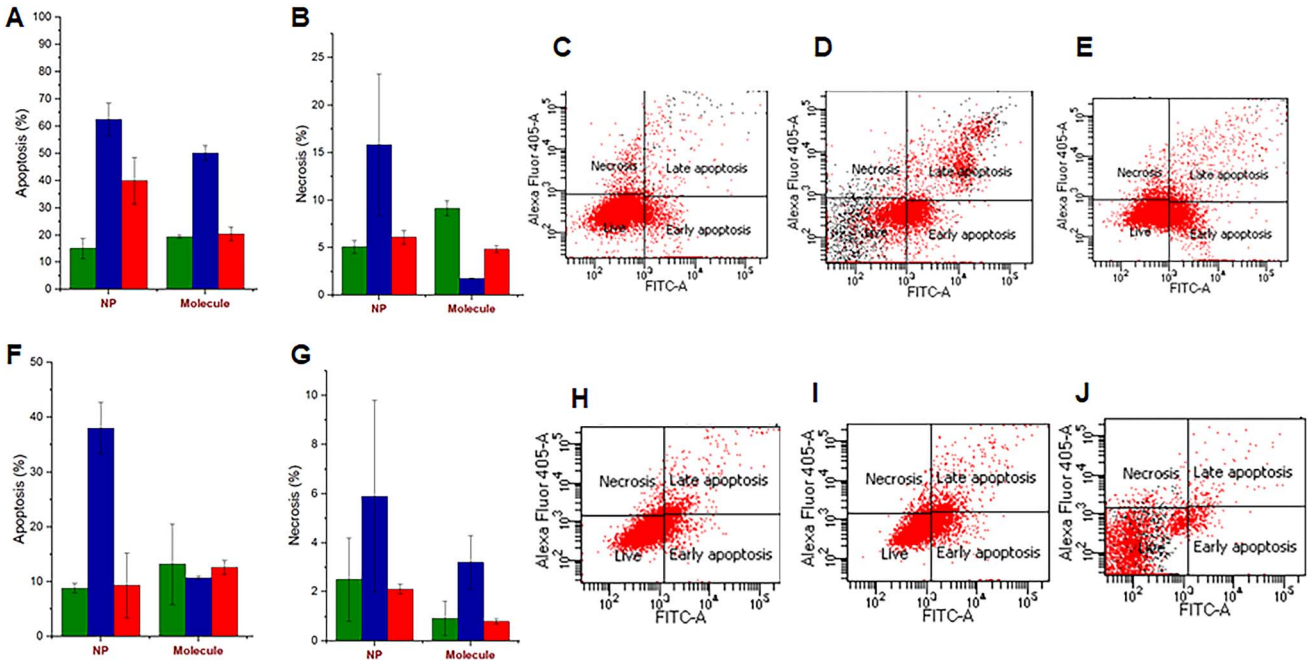

Fig. 6 Cell death mechanisms study. (A and F) Apoptosis and (B and G) necrosis in HeLa and MDA-MB-231 cells treated with **TPP**-NP (green), **ATPP**-NP (blue) and **POSSP**-NP (red). Apoptosis assay plots using annexin V for (C and H) **TPP**-NP, (D and I) **ATPP**-NP and (E and J) **POSSP**-NP in HeLa and MDA-MB-231 cells.

4. Conclusions

In this work, we have synthesized three different PNPs, **TPP**-, **ATPP**- and **POSSP**-NPs, using the co-precipitation approach. The physicochemical features of the nanoparticles were characterized by a wide range of methods. The results demonstrated the successful encapsulation of the parent porphyrin. Similar size and surface charge were obtained for the three PNPs; however, **POSSP**-NPs showed a better colloidal stability in water presumably due to the presence of POSS molecule. The PNPs showed an increase in the internalization and phototoxicity in HeLa and MDA-MB-231 cell lines as compared with their parent porphyrins as an indication of the advantages of this approach. Interestingly, despite **TPP**-NPs presenting the highest internalization, **ATPP**-NPs are the ones showing the best phototherapeutic effect, most likely due to the inherent phototoxicity associated with the parent porphyrin. The study of the cell death mechanism corroborated that cells are killed mainly through apoptosis. The trend on apoptosis is similar to the one for phototoxicity as follows **ATPP**-NPs > **POSSP**-NPs > **TPP**-NPs. Our findings suggest that encapsulating porphyrins in nanoparticles enhances their photodynamic therapy efficacy, offering a promising approach for cancer treatment.

Author contributions

Investigation: P. A. K. J, A. N., A. N., A. E., A. B., P. L.-C. Conceptualization: P. L.-C. and J. V.-E., supervision: J. V.-E., funding acquisition: J. V.-E., writing—original draft: P. A. K. J., writing—review & editing: P. A. K. J, A. N., A. N., A. E., A. B., P. L.-C. and J. V.-E.

Conflicts of interest

There are no conflicts to declare.

Data availability

Supplementary information: The data supporting this article have been included as part of the SI. See DOI: **https://doi.org/10.1039/d5ra04916d**.

Acknowledgements

Financial support was provided by the National Institute of Cancer of the National Institutes of Health under Award Number R15CA274239 (to J. L. V.-E.). The content of this publication does not necessarily reflect the views or policies of the Department of Health and Human Services, nor does the mention of trade names, commercial products, or organizations imply endorsement by the US Government. A. N. acknowledge financial support from the NanoSURE REU program, which was funded through NSF Award (DMR-2150172). The authors would like to thank Dr Jessica Shivas for their assistance with the confocal microscope.

References

1 Y. Gao, Y. Li, Z. Xu, S. Yu, J. Liu and H. Sun, *Aggregate*, 2024, **5**, e420.
2 A. Kurabayashi, H. Fukuhara, K. Furihata, W. Iwashita, M. Furihata and K. Inoue, *Cancers*, 2024, **16**, 2299.

3 D. Aebisher, I. Serafin, K. Batóg-Szczęch, K. Dynarowicz, E. Chodurek, A. Kawczyk-Krupka and D. Bartusik-Aebisher, *Pharmaceuticals*, 2024, **17**, 932.
4 H. Li, W. Xiao, Z. Tian, Z. Liu, L. Shi, Y. Wang, Y. Liu and Y. Liu, *Photodiagnosis Photodyn. Ther.*, 2023, **41**, 103236.
5 Y. Lin, T. Zhou, R. Bai and Y. Xie, *J. Enzyme Inhib. Med. Chem.*, 2020, **35**, 1080–1099.
6 I. O. Savelyeva, K. A. Zhdanova, M. A. Gradova, O. V. Gradov and N. A. Bragina, *Curr. Issues Mol. Biol.*, 2023, **45**, 9793–9822.
7 J. Han, Y. Liu, D. Peng, J. Liu and D. Wu, *Bioconjugate Chem.*, 2023, **34**, 2155–2180.
8 A. Akbar, S. Khan, T. Chatterjee and M. Ghosh, *J. Photochem. Photobiol., B*, 2023, **248**, 112796.
9 R. Chang, L. Zhao, R. Xing, J. Li and X. Yan, *Chem. Soc. Rev.*, 2023, **52**, 2688–2712.
10 Y. Wang, L. Chang, H. Gao, C. Yu, Y. Gao and Q. Peng, *Eur. J. Med. Chem.*, 2024, **272**, 116508.
11 E. Lima and L. V. Reis, *Molecules*, 2023, **28**, 5092.
12 E. Cheng, B. Li and Q. Zou, *Adv. Ther.*, 2024, **7**, 2300329.
13 F. Yang, M. Xu, X. Chen and Y. Luo, *Biomed. Pharmacother.*, 2023, **164**, 114933.
14 R. Chang, Q. Zou, L. Zhao, Y. Liu, R. Xing and X. Yan, *Adv. Mater.*, 2022, **34**, e2200139.
15 S. Li, Q. Zou, Y. Li, C. Yuan, R. Xing and X. Yan, *J. Am. Chem. Soc.*, 2018, **140**, 10794–10802.
16 H. Vadarevu, R. Juneja, Z. Lyles and J. L. Vivero-Escoto, *Nanomaterials*, 2021, **11**, 2324.
17 Z. K. Lyles, M. Tarannum, C. Mena, N. M. Inada, V. S. Bagnato and J. L. Vivero-Escoto, *Adv. Ther.*, 2020, **3**, 2000022.
18 P. Siano, A. Johnston, P. Loman-Cortes, Z. Zhin and J. L. Vivero-Escoto, *Molecules*, 2020, **25**, 4965.
19 P. Loman-Cortes, D. J. Jacobs and J. L. Vivero-Escoto, *Mater. Today Commun.*, 2021, **29**, 102815.
20 Y. Hu, J. Peng, R. Liu, J. Gao, G. Hua, X. Fan and S. Wang, *Molecules*, 2024, **29**, 6063.
21 N. K. Shee, M. K. Kim and H.-J. Kim, *Nanomaterials*, 2020, **10**, 2314.
22 X. Fu, Z. Cai, S. Fu, H. Cai, M. Li, H. Gu, R. Jin, C. Xia, S. Lui, B. Song, Q. Gong and H. Ai, *ACS Appl. Mater. Interfaces*, 2024, **16**, 27139–27150.
23 C. Li, Z. Luo, L. Yang, J. Chen, K. Cheng, Y. Xue, G. Liu, X. Luo and F. Wu, *Mater. Today Bio*, 2022, **13**, 100198.
24 W. Dai, P. Jin, X. Li, J. Zhao, Y. Lan, H. Li and L. Zheng, *Biomed. Pharmacother.*, 2023, **164**, 114881.
25 N. K. Shee, M. K. Kim and H. J. Kim, *Nanomaterials*, 2020, **10**, 2314.
26 M. Zannotti, R. Giovannetti, B. Minofar, D. Řeha, L. Plačková, C. A. D'Amato, E. Rommozzi, H. V. Dudko, N. Kari and M. Minicucci, *Spectrochim. Acta, Part A*, 2018, **193**, 235–248.
27 N. Keller, M. Calik, D. Sharapa, H. R. Soni, P. M. Zehetmaier, S. Rager, F. Auras, A. C. Jakowetz, A. Görling, T. Clark and T. Bein, *J. Am. Chem. Soc.*, 2018, **140**, 16544–16552.
28 O. Arteaga, A. Canillas, Z. El-Hachemi, J. Crusats and J. M. Ribó, *Nanoscale*, 2015, **7**, 20435–20441.
29 K. Šišková, B. Vlčková and P. Mojzeš, *J. Mol. Struct.*, 2005, **744–747**, 265–272.
30 Q. Wu, R. Xia, C. Li, Y. Li, T. Sun, Z. Xie and X. Jing, *Mater. Chem. Front.*, 2021, **5**, 8333–8340.
31 N. A. Shanazarov, A. Zare, N. M. Mussin, R. K. Albayev, A. A. Kaliyev, Y. M. Iztleuov, S. B. Smailova and A. Tamadon, *Ther. Adv. Chronic Dis.*, 2024, **15**(20406223241233206), DOI: **10.1177/20406223241233206**.
32 M. S. Afanasiev, A. D. Dushkin, T. G. Grishacheva, S. S. Afanasiev and A. V. K. Academician, *Photodiagnosis Photodyn. Ther.*, 2022, **37**, 102620.
33 H. Jin, S. Liao, F. Yao, J. Li, Z. Xu, K. Zhao, X. Xu and S. Sun, *Cancers*, 2023, **15**, 1532.
34 K. C. N. Cheung, G. M. N. Leung, R. W. K. Wu, J. W. M. Yuen, Z. Huang and E. S. M. Chu, *Photodiagnosis Photodyn. Ther.*, 2024, **46**, 104186.
35 K. Nishida, T. Tojo, T. Kondo and M. Yuasa, *Sci. Rep.*, 2021, **11**, 2046.
36 Y. E. Yegorov, K. S. Vishnyakova, X. Pan, A. E. Egorov, K. V. Popov, L. L. Tevonyan, G. V. Chashchina and D. N. Kaluzhny, *Molecules*, 2023, **28**, 1090.
37 M. G. H. Vicente, D. J. Nurco, S. J. Shetty, J. Osterloh, E. Ventre, V. Hegde and W. A. Deutsch, *J. Photochem. Photobiol., B*, 2002, **68**, 123–132.
38 S. R. Adapa, G. A. Hunter, N. E. Amin, C. Marinescu, A. Borsky, E. M. Sagatys, S. M. Sebti, G. W. Reuther, G. C. Ferreira and R. H. Jiang, *Life Sci. Alliance*, 2024, **7**, e202302547.
39 J. Wang, B. Yang, C. Lv, T. Chen, L. Sun, L. Sun, J. Hao, F. Ding, T. Wang, J. Jiang and Y. Qin, *Biomaterials*, 2022, **289**, 121812.
40 T. M. Tsubone, W. K. Martins, C. Pavani, H. C. Junqueira, R. Itri and M. S. Baptista, *Sci. Rep.*, 2017, **7**, 6734.
41 D. Samaroo, M. Vinodu, X. Chen and C. M. Drain, *J. Comb. Chem.*, 2007, **9**, 998–1011.
42 N. A. Daghastanli, R. Itri and M. S. Baptista, *Photochem. Photobiol.*, 2008, **84**, 1238–1243.
43 J. Kou, D. Dou and L. Yang, *Oncotarget*, 2017, **8**, 81591–81603.